

Nucleation of a sodium droplet on C₆₀

J. Roques^{1,2}, F. Calvo¹, F. Spiegelman¹, and C. Mijoule²

¹ *Laboratoire de Physique Quantique, IRSAMC, Université Paul Sabatier,
118 Route de Narbonne, F31062 Toulouse Cedex*

² *CIRIMAT, Université Paul Sabatier and Institut National Polytechnique,
118 Route de Narbonne, F31062 Toulouse Cedex*

We investigate theoretically the progressive coating of C₆₀ by several sodium atoms. Density functional calculations using a nonlocal functional are performed for NaC₆₀ and Na₂C₆₀ in various configurations. These data are used to construct an empirical atomistic model in order to treat larger sizes in a statistical and dynamical context. Fluctuating charges are incorporated to account for charge transfer between sodium and carbon atoms. By performing systematic global optimization in the size range $1 \leq n \leq 30$, we find that Na_nC₆₀ is homogeneously coated at small sizes, and that a growing droplet is formed above $n \geq 8$. The separate effects of single ionization and thermalization are also considered, as well as the changes due to a strong external electric field. The present results are discussed in the light of various experimental data.

PACS numbers: 61.48.+c,34.70.+e,36.40.Qv

I. INTRODUCTION

Bulk compounds of C₆₀ with alkali or alkaline earth metals can develop particularly interesting properties such as superconductivity.¹⁻⁴ At the gas phase level, the interaction between a fullerene molecule and metal atoms has attracted a significant attention, from both theoreticians⁵⁻¹⁶ and experimentalists.¹⁷⁻²⁹ Coverage of fullerenes with semiconductor atoms or clusters has also been investigated.^{30,31} For alkaline earth materials it is now commonly accepted that many atoms homogeneously surround the C₆₀ molecule in spherically centred shells. For other metals, such as lithium^{5,11,12,21} a strong charge transfer takes place with carbon and the resulting ionic interaction may be stronger than the metallic bonding. As a consequence, homogeneous coating of C₆₀ is also observed at low coverage. The same situation is seen for potassium^{6,11,18,20} and rubidium^{20,23} adsorbed on C₆₀. The adsorption of gold leads to a somewhat different picture, where the metal cluster is formed next to the fullerene.²⁸ In this case metallic bonding dominates over the partially ionic-covalent Au-C interactions.

Here we will focus on sodium, which has been the subject of a debate.^{18,26,28,29} The results of mass spectrometry measurements, and the magic numbers inferred from these measurements by the group of Martin,¹⁸ lead to the conclusion of a regular coating of C₆₀. Photoelectron spectroscopy measurements by Palpant *et al.*^{26,28} were interpreted rather similarly, these authors also providing some evidence that coating proceeds by trimers rather than monomers. On the contrary, the measurement of electric dipoles and polarizabilities by Dugourd *et al.*²⁹ seems to indicate that a segregated metal droplet is formed on the surface of the fullerene. Since the experimental conditions for the production of these clusters are similar in the three apparatus, then mainly the interpretations differ.

Up to now, there have been essentially three theoretical investigations of this problem, at least to our knowledge.^{7,9,16} The work by Rubio *et al.*⁷ assumes a complete wetting of C₆₀ by sodium with a phenomenological two-shell jellium description. This does not help much in elucidating the actual structure of Na_nC₆₀ compounds. The *ab initio* calculations by Hira and Ray,⁹ performed at the unrestricted Hartree-Fock (UHF) level, and the recent density functional theory (DFT) calculations by Hamamoto and coworkers,¹⁶ using the local density approximation (LDA), predict quite different results for the physical properties and favored structures of Na₂ on C₆₀.

In order to address this problem, we have constructed an empirical atomistic model, allowing extensive sampling of the configuration space in a wide range of sizes. In turn, this enhanced sampling enables one to achieve unconstrained global optimization as well as dynamical and finite temperature studies.

For this model to be physically and chemically realistic, we first carefully performed first-principles calculations of the binding of Na and Na₂ on C₆₀. These calculations, described and discussed in the next section, are converted into a suitable set of parameters for our model, as fully described in Sec. III. The main results can be separated into five categories, which will be presented in the following order. After describing the most stable structures found with the present model, and some of their properties, we discuss the distinct effects of charging and thermalizing the clusters, and the possible influence of a strong external electric field. The diffusion dynamics of the metal atoms over the C₆₀ surface is also discussed. The main results are summarized and discussed in Sec. V, in the light of the various experimental and theoretical works available. A tentative rationalization for the apparently contradictory observations is proposed.³²

II. FIRST-PRINCIPLES CALCULATIONS

A. Methods

Density functional theory calculations have been used to provide reference data for the interactions between a fullerene molecule and one or two sodium atoms. The B3LYP hybrid method proposed by Becke³³⁻³⁵ and included in the GAUSSIAN98 package³⁶ was used. This method is a mixture of Hartree-Fock and DFT exchange terms associated with the gradient corrected correlation functional of Lee *et al.*³⁷ Calculations were made using LANL2DZ basis sets proposed by Hay *et al.*³⁸ where the double-zeta quality was used for the carbon all-electron calculations while effective core potentials were used for sodium atoms to replace the ten inner electron cores. For these atoms the valence electrons were described with double zeta quality basis sets proposed by the same authors.

The first part of our calculation focussed on the adsorption of a single exohedral Na atom on the C₆₀ molecule. The DFT-LDA calculations performed by Hamamoto and coworkers¹⁶ showed that the geometry of C₆₀ does not change significantly during the full geometrical optimization of Na_nC₆₀ (with $1 \leq n \leq 12$), compared to the case of pure C₆₀. So, in the present study, the fullerene was frozen at its optimized geometry and, for NaC₆₀ and Na₂C₆₀, only the positions of the alkali atoms were relaxed. We can distinguish two kinds of CC bond lengths in the C₆₀ molecule. The simple C-C and the double C=C bonds used in this study were respectively frozen at 1.45 Å and 1.37 Å, close to the experimental values of Hedberg *et al.*³⁹

B. Adsorption of a single alkali atom on C₆₀

We label H the adsorption site located above the center of an hexagonal site, P the site above a pentagon, BHH above the double C=C bond, BHP above the single C-C bond, and finally T above one carbon atom (vertex). In each case, only the radial distance d from the alkali atom to the centre of C₆₀ was optimized. The adsorption energies (E_a) of p sodium atoms on C₆₀ were calculated from the equation:

$$E_a = E(\text{C}_{60}) + p \times E(\text{Na}) - E(\text{Na}_p\text{C}_{60}). \quad (1)$$

Different spin multiplicities were checked in order to get the most stable ground state.

The adsorption energy, equilibrium distance, charge transferred and dipole moments are presented in Table I for the five adsorption sites. As can be seen, H and P are the most stable configurations with a small preference of only 0.03 eV for the hexagon.

TABLE I: Adsorption energies E_a , equilibrium distances Na-C, Mulliken charges on the alkali atom, and dipole moment of NaC₆₀. The present values are given in bold face.

Adsorption site	E_a (eV)	Na-C (Å)	q/e	μ (D)
H	0.65 / 0.10 ^a 2.10 ^b	2.74 / 5.08 ^a 2.69 ^b	0.87 / 1.07 ^b	14.53 / 14.63 ^b
P	0.62 / 0.10 ^a 2.05 ^b	2.70 / 5.18 ^a 2.70 ^b	0.87 / 1.06 ^b	15.60 / 15.80 ^b
BHH	0.58 / 0.10 ^a 1.93 ^b	2.59 / 5.00 ^a 2.47 ^b	0.87 / 1.05 ^b	17.08 / 16.54 ^b
BHP	0.55 / 0.10 ^a 1.78 ^b	2.53 / 5.00 ^a 2.46 ^b	0.85 / 1.06 ^b	16.32 / 16.48 ^b
T	0.52 / 0.10 ^a 1.98 ^b	2.47 / 4.50 ^a 2.39 ^b	0.85 / 1.04 ^b	16.98 / 17.10 ^b
				16.3 ± 1.6 ^c

^aUnrestricted Hartree-Fock calculations [8]

^bDFT-LDA calculations [16]

^cExperimental data [29,40]

These results are in agreement with the calculations performed by Hamamoto *et al.*¹⁶ who found H as the most stable configuration with a weak difference between H and P of about 0.05 eV. However, the adsorption energies reported in Ref. 16 are between 1.23 and 1.45 eV higher than ours. Since in both calculations double zeta basis sets were used, this difference is certainly due to the use of the local density approximation in the latter work. This approximation is known to often strongly overestimate adsorption energies.⁴¹ In contrast, Hira and Ray⁸ performed unrestricted Hartree-Fock calculations of NaC₆₀ and predicted a very weak adsorption energy of only 0.10 eV with no energy difference between the five different sites. Bond sites configurations, which are probably not true minima, show a small preference of 0.03 eV for the C=C bond, in agreement with the findings by Hamamoto and coworkers.¹⁶

The less stable of the 5 configurations corresponds to the vertex site, indicating that the adsorption of a single alkali atom is favored by a maximal coordination.

Estimates of the barrier for diffusion of Na over C_{60} can be made from the data in Table I. We find barriers of 0.07 eV between H sites or between P sites, and 0.07 and 0.10 eV between H and P sites. Thus we can expect a significant mobility at room temperature, and a possible influence of temperature on the average location of sodium atoms.

The net charge on the alkali atom, as estimated from a Mulliken population analysis,⁴² is also given in Table I. Our results are consistent with experimental^{18,28,40} and other theoretical^{8,16} studies, which predicted an electronic transfer of about one electron from the singly occupied atomic orbital of the alkali atom to the lowest-unoccupied molecular orbital (LUMO) of C_{60} . This behavior indicates a significant ionic bonding of the alkali atom with the fullerene. In the unrestricted Hartree-Fock calculations performed by Hira and Ray,⁸ no significant electronic transfer between Na and C_{60} was observed. This is correlated with a large distance (larger than 4.5 Å) between Na and C_{60} , and no actual bonding.

The optimized bond lengths between the alkali atom and the nearest carbon atom calculated using the nonlocal functional are listed in Table I. These values show a decrease from H to P, then BHH and BHP, and finally to T sites. Thus the Na–C distance somewhat also reflects Na coordination.

Finally, the dipole moments are given in Table I for all five configurations. Their values range from 14.53 D for site H to 17.08 D for site BHH. They agree well with the experimental data by Antoine *et al.*,⁴⁰ who reported a dipole moment of 16.3 ± 1.6 D. Our results are also in good agreement with the DFT-LDA calculations of Hamamoto and coworkers.¹⁶

C. Adsorption of two alkali atoms on C_{60}

We are now interested in the relative position of two alkali atoms adsorbed on the C_{60} molecule. From results of the previous part (strong electronic transfer from alkali atom to C_{60} molecule and weak diffusion barrier on the C_{60} surface), we can expect that two alkali atoms will undergo a strong electrostatic repulsion. Two configurations were selected, with two adjacent sites or two opposite sites, respectively. Since the H sites are the most stable in the case of a single atom, we have restricted the present study to hexagonal sites only. In the case of opposite sites, only the radial distance to C_{60} was optimized. For adjacent sites, the Na–Na distance was also optimized.

TABLE II: Adsorption energies E_a , equilibrium distances Na–C and Na–Na, Mulliken charges on each alkali atom, and dipole moment of Na_2C_{60} .

Adsorption site	E_a (eV)	Na–C (Å)	Na–Na (Å)	q/e	μ (D)
adjacent	0.98	2.55	4.46	0.83	23.75
opposite	1.31 / 0.24 ^a 4.09 ^b	2.72 / 4.48 ^a		0.85 / 1.05 ^b	0

^aUnrestricted Hartree-Fock calculations [9]

^bDFT-LDA calculations [16]

The adsorption energies for Na_2C_{60} [Eq. (1)] are given in Table II. For the two configurations, adsorption energies are given along with the optimized Na–C and Na–Na distances, Mulliken charges on each alkali atom, and the associated dipole moment. The most stable configuration turns out to be the one with opposite sites, lower by about 0.34 eV than the other one. Even though the Mulliken charges on sodium are slightly smaller, they remain comparable to the single atom case. This significant electronic transfer (about 0.85e per atom) causes a strong electrostatic repulsive interaction between Na atoms, which in turn destabilizes the adjacent configuration. The present result is consistent with the DFT-LDA calculations of Hamamoto *et al.*,¹⁶ and with the experimental interpretations by Martin *et al.*¹⁸ for clusters with fewer than 7 sodium atoms.

III. EMPIRICAL MODELLING

The calculations presented in the previous section will now be used to parameterize an atomistic model, in order to achieve large scale sampling of the configuration space of larger clusters and perform simulations, which are even today beyond the possibilities of *ab initio* approaches.

A. Fluctuating charges potential

The crucial element determining the relative extents of ionic-covalent forces and metallic forces is charge transfer between carbon and sodium. This transfer is expected to depend on how the metal atoms are located over C_{60} . For instance, atoms closest to the C_{60} surface are likely to undergo a stronger charge transfer than the most distant ones. Therefore we cannot use a model with fixed partial charges. A convenient answer to this problem is provided by the fluctuating charges model, often denoted as “fluc-q” potential. Originating from DFT analyses,⁴³ these ideas have been simultaneously but independently applied to a variety of diatomic molecules and some peptides by Rappé and Goddard,⁴⁴ as well as multicharged metal clusters by Sawada and Sugano.⁴⁵ More recently, the group of Berne⁴⁶ has suggested how to improve molecular dynamics simulations with fluc-q potentials by using extended Lagrangian techniques, in a fashion similar to the Car-Parrinello method.⁴⁷ More rigorous derivations from density functional theory have since been proposed,^{48,49} and also a treatment within hybrid quantum mechanical/molecular mechanical models.⁵⁰ The latest developments include higher-order electrostatic terms such as dipoles,⁵¹ and the treatment of polarization forces.⁵² Fluc-q potentials have been used by Ribeiro to study the dynamics in the glass-forming liquid $Ca_{0.4}K_{0.6}(NO_3)_{1.4}$ ⁵³ as well as the Chemla effect in molten alkali nitrates.⁵⁴

Let us denote by $\mathbf{R} = \{\mathbf{r}_i, \mathbf{r}'_j\}$ the geometry of the Na_nC_{60} system, the vectors \mathbf{r}_i and \mathbf{r}'_j representing the 3-dimensional positions of the n sodium atoms and 60 carbon atoms, respectively. We assume that the whole cluster carries a total charge Q , which may not necessarily be zero. The total potential energy V of the system is written as the sum of several contributions:

$$V(\mathbf{R}) = V_{Na}(\{\mathbf{r}_i\}) + V_C(\{\mathbf{r}'_j\}) + V_{inter}(\mathbf{R}) + V_{Coul}(\mathbf{R}). \quad (2)$$

V_{Na} is the pure metallic binding energy, which we took as an empirical many-body potential in the second moment approximation (SMA) to the electronic density of states in the tight-binding theory.⁵⁵ This potential involves five parameters ξ_0 , ε_0 , p , q , and r_0 :

$$V_{Na}(\{\mathbf{r}_i\}) = \varepsilon_0 \sum_{i < k} e^{-p(r_{ik}/r_0 - 1)} - \sum_i \left[\xi_0^2 \sum_{k \neq i} e^{-2q(r_{ik}/r_0 - 1)} \right]^{1/2} \quad (3)$$

In this equation, the sum runs over all sodium atoms, and r_{ik} is the usual distance between atoms i and k . The initial values for the five parameters were taken from Ref. 56. V_C is the pure covalent binding energy of the C_{60} molecule. This term was modelled with the Tersoff potential.⁵⁷ We did not attempt to change any of the original parameters, but we added several fixed point charges to improve the electrostatic description of this molecule. Following Schelkacheva and Tareyeva,⁵⁸ 60 charges $+\delta q$ were placed on each C atom, while 30 charges $-2\delta q$ were placed at the center of each C=C bond. Actually the full Tersoff potential is relatively costly, and we only used it for reoptimizing some stable structures. In the next section, the effects of approximating C_{60} as rigid will be quantitatively addressed.

The term V_{inter} represents the non-ionic part of the interaction between carbon and sodium atoms. It is simply approximated as a pairwise repulsion, involving 2 new parameters D and β :

$$V_{inter}(\mathbf{R}) = \sum_{i \in Na_n} \sum_{j \in C_{60}} D e^{-\beta r_{ij}}. \quad (4)$$

We will assume in the following that chemical bonding between Na and C is controlled by charge transfer, hence we neglect other effects such as dispersion forces. In the fluc-q model, the Coulomb electrostatic interaction is expressed as

$$\begin{aligned} V_{Coul}(\mathbf{R}) = & \sum_i \left[\varepsilon_{Na} q_i + \frac{1}{2} H_{Na} q_i^2 \right] + \sum_j \left[\varepsilon_C q'_j + \frac{1}{2} H_C q'^2_j \right] \\ & + \sum_{i,j} J_{ij} q_i q'_j + \sum_{i < i'} J_{ii'} q_i q_{i'} + \sum_{j < j'} J_{jj'} q'_j q'_{j'}, \end{aligned} \quad (5)$$

where q_i and q'_j denote the charges carried by sodium atom i and carbon atom j , respectively. In Eq. (5) the labels (i, i') and (j, j') refer to sodium and carbon, respectively. ε_{Na} and ε_C are the electronegativities, H_{Na} and H_C the hardnesses, and J_{ij} the Coulomb interactions, which are assumed to be explicit in the interatomic distance r_{ij} . In practice, we have chosen the Ohno representation.⁵⁹

$$J_{ij}(r) = [r^2 + H_{ij}^{-2} \exp(-\gamma_{ij} r^2)]^{-1/2}. \quad (6)$$

For a given geometry \mathbf{R} , the effective electronegativities of each atom are defined by $\varepsilon = \partial V / \partial q$, which yields

$$\varepsilon_i = \varepsilon_{\text{Na}} + H_{\text{Na}} q_i + \sum_j J_{ij} q'_j + \sum_{i' \neq i} J_{ii'} q_{i'} \quad (7)$$

for sodium atoms, and a similar equation for carbon atoms. Following Sanderson,⁶⁰ we now use the principle of electronegativity equalization. This principle states that, at equilibrium, all ε 's are the same in the molecule. If we denote by λ this common value, then the charges $\{q_i, q'_j\}$ are such that they minimize the potential V_{Coul} above, under the constraint that the total charge is prescribed to a specific value Q . This minimization is equivalent to adding the extra term $\lambda(\sum_i q_i + \sum_j q'_j - Q)$ to the potential V_{Coul} , and thus λ plays the role of a Lagrange multiplier.

Finding the optimal charges amounts to solving a $(n + 61) \times (n + 61)$ linear system. This system has a unique solution, as long as the hardnesses are all strictly positive. Otherwise the quadratic form V_{Coul} could no longer be minimized.

We did not attempt to refine the present model further by adding higher order electrostatic or polarization terms and we assume that the self-consistency of charges is sufficient to ensure a correct electrostatic balance. Dispersion forces have been neglected as well. The interested reader is referred to the works in Refs. 51 and 52 for more details. However, we should mention that the fixed charges $(\delta q, -2\delta q)$, denoted as q_k in what follows, contribute to a better electrostatic description for the whole system. The fluc-q potential can easily account for such extra fixed charges as well as for a possible external electric field \mathbf{E} . Both fixed charges and electric field affect the self-consistent determination of the fluctuating charges, and the potential V_{Coul} should be supplemented with the term

$$\sum_{i,k} J_{ik} q_i q_k + \sum_{j,k} J_{j,k} q'_j q_k + \sum_i (\mathbf{E} \cdot \mathbf{r}_i) q_i + \sum_j (\mathbf{E} \cdot \mathbf{r}_j) q'_j. \quad (8)$$

B. Parameterization

The empirical fluc-q potential described in the previous paragraph has 15 parameters, namely the five parameters of the SMA potential, the two parameters of the Na-C repulsion, the electronegativity difference $\varepsilon_{\text{C}} - \varepsilon_{\text{Na}}$, the six parameters γ_{ij} and H_{ij} , which include the two hardnesses H_{Na} and H_{C} , and finally the fixed charge δq . These parameters were chosen so as to reproduce several properties previously computed by DFT calculations, or measured in experiments. However these data do not give much insight into the bonding between Na and C atoms. In addition, some of the parameters, especially those involved in the $J_{ij}(r)$ functions, can be in principle extracted from calculations on diatomic molecules only. Also, while Na_2 and C_2 are well characterized experimentally and theoretically, almost no data is available for the NaC molecule.

We have therefore achieved *ab initio* Configuration Interaction (CI) calculations of NaC, as well as some calculations on Na_2 and C_2 to get the Coulomb integrals. These were taken in minimal linear combinations of atomic orbitals basis set obtained by contracting the Gaussian-type orbitals of atomic self-consistent field calculations in the previous basis sets. The pointwise integrals were then fitted through the Ohno functions, Eq. (6) above. The *ab initio* calculations on Na_2 also provided estimates of the binding energy and equilibrium distance that should be predicted by the model.

TABLE III: Data used for fitting the empirical model with fluctuating charges.

Property	Source	Reference	Predicted
q/e (NaC_{60})	B3LYP	0.87	0.88
μ (NaC_{60} , D)	B3LYP	14.5	14.5
ΔE (Na_2C_{60} , eV)	B3LYP	-0.34	-0.27
$r(\text{Na}_2, \text{\AA})$	<i>ab initio</i> ^a	3.06	3.34
$E(\text{Na}_2, \text{eV})$	<i>ab initio</i> ^a	0.74	0.58
$\alpha(\text{C}_{60}, \text{\AA}^3)$	exp. ^b	76.5	58.5

^aData from Jeung, Ref.⁶¹.

^bData by Antoine *et al.* from Ref. 62

Appropriate fits of the Coulomb integrals gave us initial guesses for the parameters γ_{ij} and H_{ij} . We then obtained the whole set of parameters by minimizing a standard error function χ^2 , to reproduce the following quantities, quoted in Table III:

1. the charge transfer from sodium ($0.87e$) and the electric dipole (14.5 D) in NaC_{60} , values taken from our DFT calculations;
2. the energy difference between the two Na_2C_{60} isomers with sodium atoms on adjacent or opposite hexagonal sites ($\Delta E = -0.34$ eV from our DFT calculations, in favor of the opposite sites location);
3. the binding energy (0.74 eV) and equilibrium distance (3.06 Å) in Na_2 from *ab initio* calculations;⁶¹
4. the experimental electric polarizability of C_{60} (76.5 \AA^3 , taken from Ref. 62).

The error function χ^2 was then minimized using a local Monte Carlo search. The moves in the parameters space were not taken too large, in order to keep the parameters close to their initial magnitudes. The final values of the parameters of the SMA potential are $\varepsilon_0 = 0.01366$ eV, $\xi_0 = 0.1689$ eV, $p = 7.175$, $q = 1.34$, and $r_0 = 3.29$ Å. The parameters for the repulsive potential between Na and C atoms are $D = 313.4$ eV and $\beta = 3.423 \text{ \AA}^{-1}$. For the Coulomb integrals, we found $H_{\text{Na}} = 7.16$ eV, $H_{\text{C}} = 13.68$ eV, $H_{\text{NaC}} = 6.32$ eV, $\gamma_{\text{Na}} = 0.129 \text{ \AA}^{-2}$, $\gamma_{\text{C}} = 1.02 \text{ \AA}^{-2}$, and $\gamma_{\text{NaC}} = 0.15 \text{ \AA}^{-2}$. Finally, the electronegativity difference was taken as $\Delta\varepsilon = 4.6$ eV, and the fixed charge δq as 0.209. We represented in Fig. 1 the Coulomb interactions between Na and C atoms. They are found to remain very close to the *ab initio* calculations.

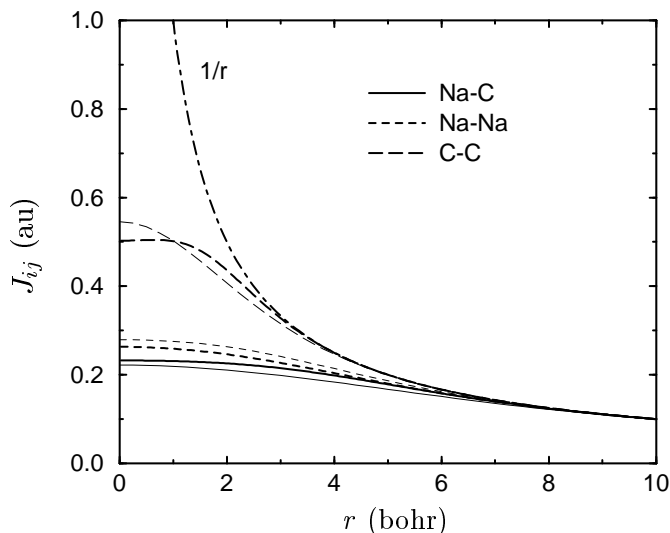


FIG. 1: Coulomb integrals for the Na_2 , C_2 and NaC molecules. The curves are given for the empirical potential (thick lines) and for the *ab initio* calculation (thin lines).

The predicted values of the quantities used in the fitting procedure are also reported in Table III. The general consistency is very good, even though we note that the polarizability of C_{60} is slightly underestimated in our model. However, only the δq parameter has some influence on this parameter. The energy difference between the two isomers of Na_2C_{60} is somewhat overestimated, but the crucial point here is that the isomers are ordered similarly.

C. Simulation tools

The putative global minima, or lowest energy structures, were determined using a variant of the Monte Carlo+minimization algorithm,⁶³ also known as basin-hopping.^{63,64} This optimization stage was made with a fully rigid C_{60} molecule, and the random atomic displacements of the sodium atoms were of two kinds. With a probability p , the selected atom is moved from its equilibrium position by a vector $\Delta\mathbf{r}$ with maximum amplitude 10 Å. With probability $1 - p$, it is moved anywhere over the C_{60} with the same radial distance from the centre of mass of the fullerene. In practice, all sodium atoms are moved before a quench is performed to find a new stable minimum. The value of p was taken as 80% for the smaller sizes, and decreased down to 10% for $n > 12$. To prevent divergences in the fluc-q potential due to short distances resulting from the random displacements, and to prevent pathological crossing of the C_{60} surface by Na atoms, we added a purely repulsive potential between the surface of C_{60} and the sodium atoms:

$$V_{\text{rep}}(\{\mathbf{r}_i\}) = \sum_i \frac{\kappa}{2} (\|\mathbf{r}_i\| - r_{\text{C}_{60}})^2, \quad (9)$$

where we took $\kappa = 880 \text{ eV}/\text{\AA}^2$ and $r_{C_{60}} = 3.89 \text{ \AA}$. This potential was only used in concern with global optimization.

We also carried out some finite temperature molecular dynamics simulations using the Nosé-Hoover chain thermostat technique.⁶⁵ In the extended Lagrangian scheme, the charges were also thermostatted at a low temperature $T^* = T/100$, T being the vibrational temperature, to prevent divergence of their kinetic temperature.⁶⁶ The masses of the thermostats were taken as $Q_i = 3nk_B T/\omega^2$ (1st thermostat) and $Q_{k>1} = Q_1/3n$ (other thermostats) for the atoms, and $Q_1^* = (n+60)k_B T^*/\omega_0^2$ (1st thermostat) and $Q_{k>1}^* = Q_1^*/(n+60)$ (other thermostats) for the charges.⁶⁵ Appropriate values for the square frequencies were taken as $\omega^2 = 10^{-6}$ and $\omega_0^2 = 5 \times 10^{-6}$ atomic units, respectively. The fictitious masses of the charges were chosen equal for all charges, and taken as 10^3 au. The velocity Verlet algorithm was used to propagate the dynamics with a time step $\Delta t = 1$ fs, and the parallel tempering strategy⁶⁷ was used to accelerate convergence when simulating the clusters at thermal equilibrium.

IV. RESULTS

A. Structural properties

For each size n in the range $1 \leq n \leq 30$, 10^4 quenches were performed during the basin-hopping searches for the global minimum. The most stable structures found using this algorithm are reported in Fig. 2. We have also indicated the (non- C_1) symmetry groups. Although this may not be obvious from looking at Fig. 2, the C_{60} molecule is also optimal in these structures when modelled with the Tersoff potential.⁵⁷ The effect of adding sodium atoms on the C_{60} geometry will be quantified later.

At low coverage, Na atoms tend to stay as far as possible from each other, in order to minimize Coulomb repulsion induced by a significant charge transfer. The growth roughly goes symmetric until the seventh atom is added. There are then only few open spaces for the eighth atom to stay, and the structure found by breaking some Na–C bonds in favor of metal Na–Na bonds appears slightly more stable. More importantly, this droplet initially created for $n = 8$ remains at larger sizes and grows monotonically as further atoms are deposited. Actually the droplet even captures some of the isolated atoms during the growing process: only two atoms remain isolated for $n = 30$.

These are the main results of the present work. Our model predicts that charge transfer is initially strong enough to inhibit metallic bonding. Then, as more atoms are added, the competition between ionic and metal forces finally turns at the advantage of the latter. The crossover size for this wetting-to-nonwetting' transition, which we estimate here to be around $n = 8$, may be of course somewhat different in more accurate chemical descriptions. It is however worth pointing out that, even though the present potential is not explicitly quantal, it still shows an enhanced stability of Na trimers upon nucleation. The atom unconnected to the C_{60} carries a slightly negative charge, and the whole trimer nearly has the charge +1, in agreement with the known special stability of Na_3^+ .⁶⁸

In Fig. 3 we have plotted two indicators of the mistake made when considering the C_{60} molecule as rigid. The whole Na_nC_{60} systems were locally reoptimized using the Tersoff potential, and we calculated the relative error $e = [A(\text{rigid}) - A(\text{Tersoff})]/A(\text{Tersoff})$ for two properties A : (1) the global shape is estimated from $A = \sum_i \|\mathbf{r}_i\|^2$, where the sum runs over all Na and C atoms, and (2) the total charge carried by sodium atoms, $A = \sum_{i \in \text{Na}} q_i$.

As can be seen in Fig. 3, the relative error remains smaller than 5×10^{-4} for the shape, and smaller than 2×10^{-4} for the charge. Of course, heating the cluster would introduce some degree of floppyness in the fullerene. However, at the temperatures involved in the experiment (the order of magnitude of 300 K), we do not really have to worry about the vibrational motion of carbon atoms. The C_{60} molecule itself only melts above 2000 K.⁶⁹ Hence it is quite safe to use the rigid approximation in the present work. We note, however, that other materials such as fluorine may spontaneously induce significant deformations when they cover C_{60} in large amounts.⁷⁰

B. Electrostatics

The fluctuating charges potential can be straightforwardly used to compute electrostatic properties, some of them being amenable to experimental comparison. The total charge carried by all sodium atoms is represented in Fig. 4 versus cluster size. As long as new hexagonal sites of C_{60} are capped by the added Na atoms, charge transfer increases steadily. The total charge reaches a plateau at $n = 8$, corresponding to the onset of nucleation. Above this size, slightly more than 3 electrons are transferred in the present empirical model. Single point DFT calculations performed on some of the smaller sizes confirm this trend, but they estimate the maximal charge transfer to be closer to 5–6 rather than 3. Such a larger value is in agreement with the theoretical findings of Hamamoto and coworkers.¹⁶ This may

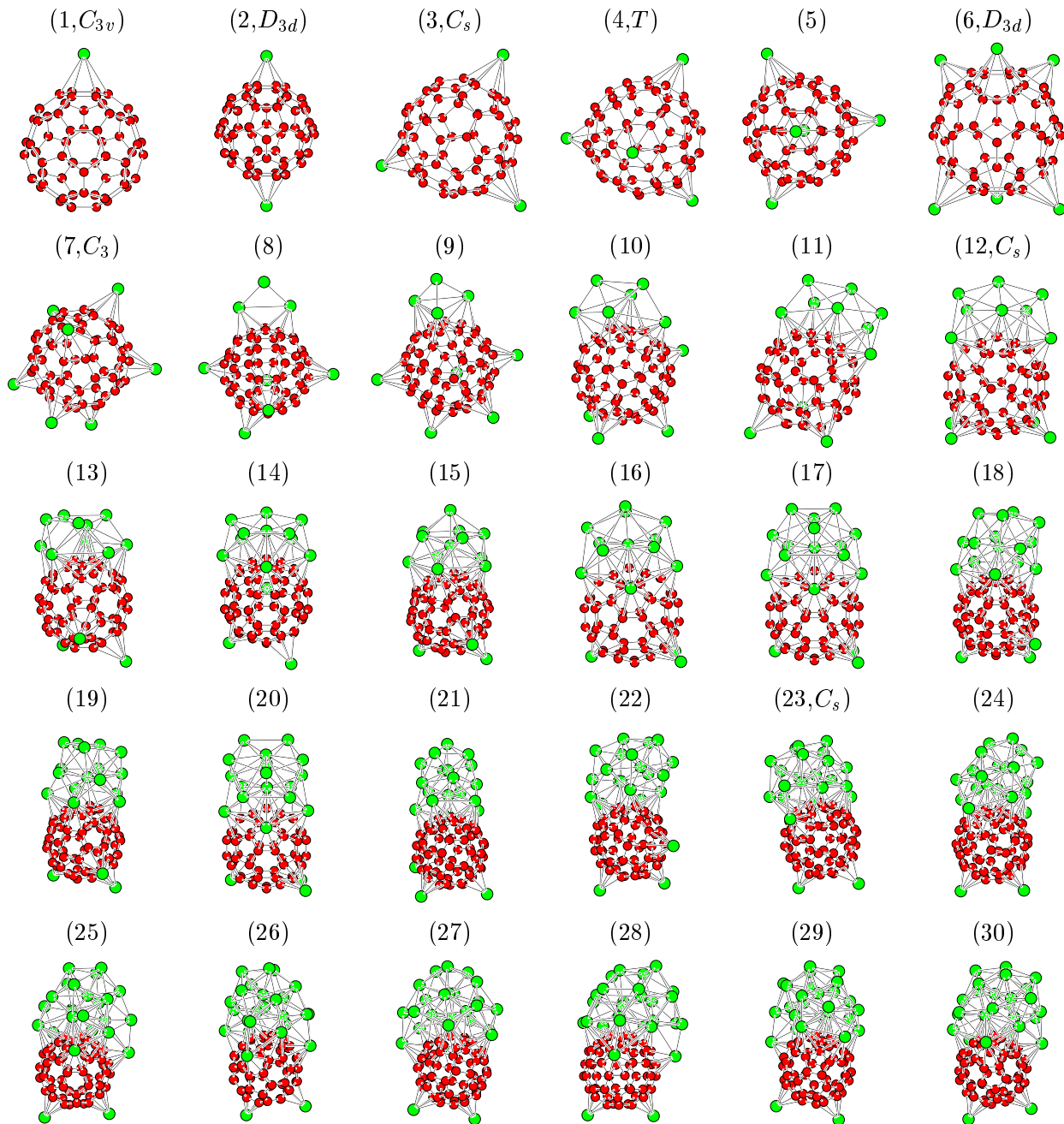


FIG. 2: Lowest-energy structures found for Na_nC_{60} in the range $1 \leq n \leq 30$ using the fluctuating charges potential.

be associated with the role in the molecular orbital calculations of the threefold degenerate LUMO orbital of C_{60} , an effect which cannot be explicitly accounted for in the present continuous electrostatic model.

In Fig. 4 we also plotted the variations of the magnitude of the electric dipole moment μ . Two different regimes are again observed, that can be correlated with the known structural transition. Below 8 sodium atoms, the rather symmetric structures due to Coulomb repulsion exhibit some odd-even alternance in the dipole. From $n = 8$ and beyond, the growing droplet shows a much more progressive increase of the dipole, except close to sizes that lose one of the isolated atoms.

The zero temperature electric polarizability α was calculated by averaging the diagonal part of the corresponding 3×3 tensor. Small electric fields (10^{-6} au) were added along the three Cartesian axes, and the dipoles were obtained after reoptimization. At finite temperature corresponding to the experiments by Dugourd *et al.*,²⁹ we estimated the electric susceptibility χ by assuming that the dipoles were rigid and statistically oriented within the electric field. This allows us to use a simple Langevin formula for the susceptibility, namely $\chi = \alpha + \mu^2/3k_B T$. The variations of α

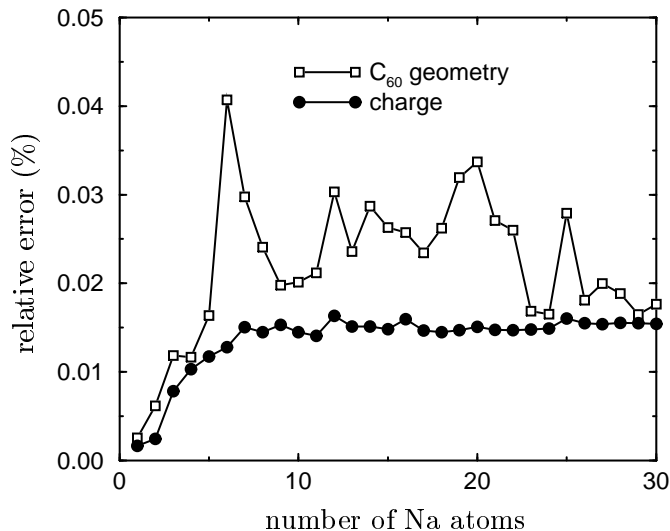


FIG. 3: Relative error for the geometric distortion (empty squares) and for the total charge on sodium (full circles) when considering the C₆₀ molecule as rigid, with reference to the Tersoff potential.

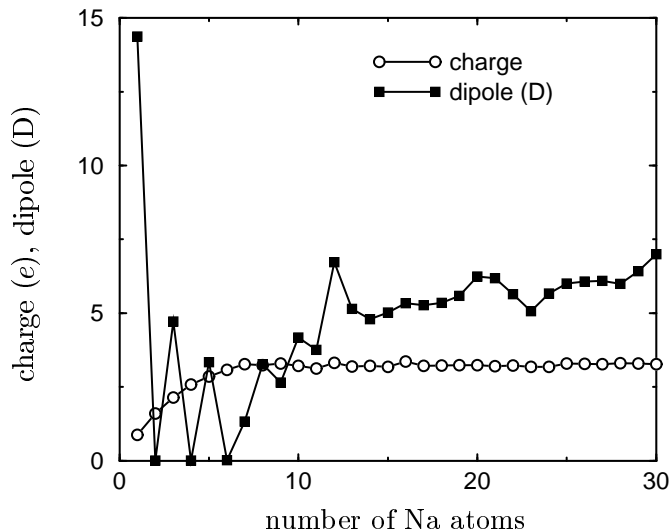


FIG. 4: Total charge (empty circles) and electric dipole moment (full squares) versus size in Na_nC₆₀ clusters.

and $\chi(300\text{ K})$ with size are represented in Fig. 5 for the entire range $1 \leq n \leq 30$.

The polarizability shows no particular dependence with n besides a steady but slow increase. On the contrary, because μ has large variations with size, this also holds for χ . Experimental data²⁹ are in semi-quantitative agreement with the present results. While the general behavior observed by Dugourd *et al.*²⁹ is similar to the one for χ in Fig. 5, the values they measure are significantly larger. This might be due to the neglect of probable increases in μ as temperature increases, due to the floppiness of these clusters at 300 K.

C. Charge and temperature effects

In experiments, clusters are ionized for subsequent size-selection. To see the general influence of ionization on the growing process of Na clusters over C₆₀, we have performed additional global optimization on anionic ($Q = -1$) and cationic ($Q = +1$) systems. The size of the largest sodium fragment is represented in Fig. 6 versus the total number of sodium atoms. Here a fragment is a set of connected atoms, where any two atoms are said to be connected whenever they are distant by less than 8 bohr. This quantity is suitable for detecting the onset of nucleation. Indeed, we can

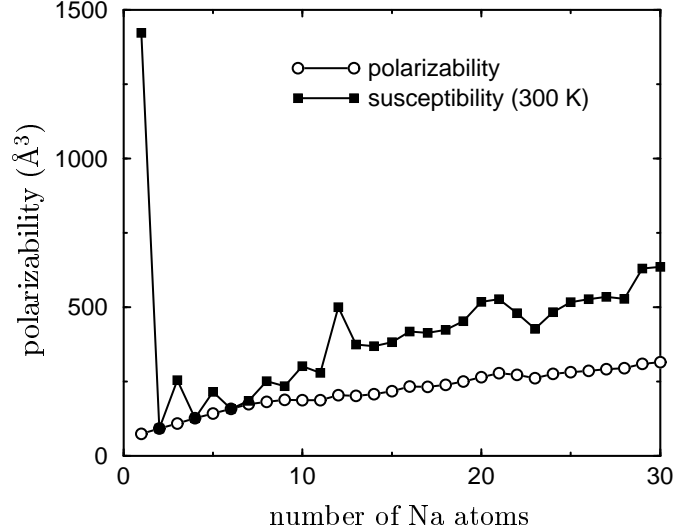


FIG. 5: Electric polarizability (empty circles) and susceptibility at 300 K (full squares) versus size in Na_nC_{60} .

easily identify in Fig. 6 the sizes of neutral clusters where the droplet captures one of the remaining isolated atoms. These sizes are found for $n = 13, 18,$ and 22 .

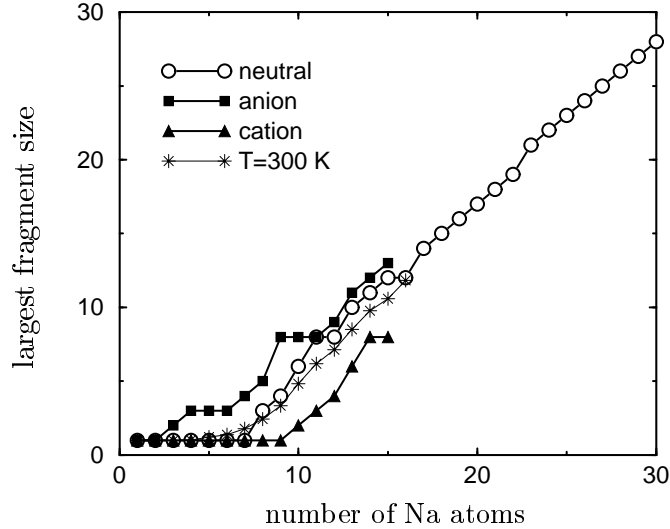


FIG. 6: Size of the largest fragment in neutral (empty circles), anionic (full circles, $Q = -1$), cationic (full triangles, $Q = +1$) $\text{Na}_n\text{C}_{60}^Q$ clusters. The average value at 300 K calculated from simulations is also given as stars.

Cationic clusters are less stable than neutrals, as they start to nucleate a droplet only above $n = 9$. This should be attributed to the larger coulombic repulsion the new atoms undergo as they are placed close to already present atoms. On the contrary, charging negatively the system diminishes charge transfer on sodium and therefore helps in creating metallic bonds. This is precisely what we see in Fig. 6, where the crossover size between coating and segregation is only 3. Obviously, the above arguments should be further discussed in the light of quantum effects.

The finite temperature equilibrium properties have been simulated using constant temperature, extended Lagrangian molecular dynamics as described in the previous section. The simulations were carried out for 30 simultaneous temperatures equidistant by $\Delta T = 10$ K, and were each 10 ns long, after 2 ns were initially discarded for equilibration. To prevent the alkali atoms from dissociating at high temperatures, we enclosed the whole system inside a spherical container centered around the C_{60} .

The time averaged size of the largest fragment is also represented in Fig. 6, at $T = 300$ K, for $1 \leq n \leq 30$. This quantity essentially follows the 0 K behavior, but is slightly higher than 1 for $n = 6$ and 7 . For $n \geq 8$, the 300 K value is slightly lower than the static value. This suggests that some metallic bonds are weak and easily broken for larger

droplets. One must then recall that 300 K is quite a large temperature for sodium clusters, and that dissociation events would tend to occur on the droplet if there were no artificial container to prevent it.

The influence of the fullerene on the global finite-temperature behavior of the sodium cluster was investigated by calculating the heat capacity of $\text{Na}_{20}\text{C}_{60}$, and comparing to our previous results on bare Na clusters.⁷¹ The thermodynamical data was analysed using a multiple-histogram reweighting procedure.⁷² The heat capacity curves are given in Fig. 7, and we also represented the variations of the (arithmetic) average fragment size $\langle n \rangle$ with increasing temperature.

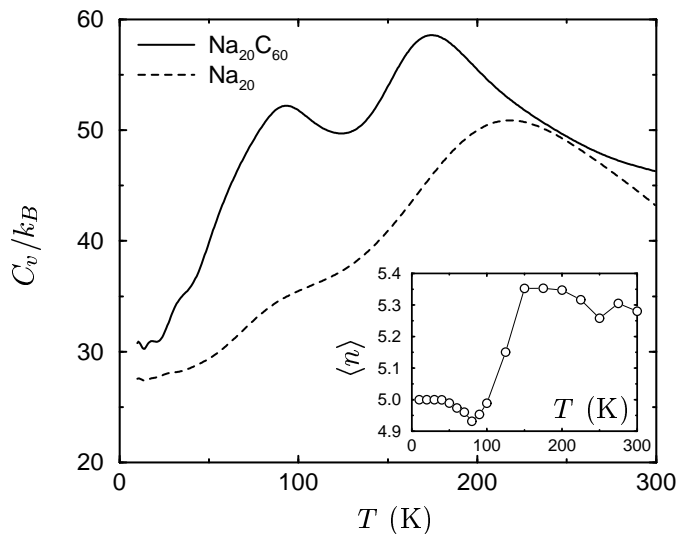


FIG. 7: Heat capacities of Na_{20} in gas phase or deposited on C_{60} . Inset: average fragment size $\langle n \rangle$ versus temperature in $\text{Na}_{20}\text{C}_{60}$.

The heat capacity of $\text{Na}_{20}\text{C}_{60}$ looks slightly different from that of Na_{20} , with an extra shoulder near 40 K. The main features at ~ 100 K and ~ 200 K in the bare cluster are enhanced in the supported cluster. Looking at snapshots of configurations taken from the $T = 50$ K trajectory indicates that some sodium atoms can change adsorption sites, especially isolated ones. The peak at 100 K can be correlated with preliminary isomerization of the Na_{17} droplet, from which some atoms can dissociate while skating over the C_{60} surface. This is best evidenced on the small decrease of $\langle n \rangle$ with T . On the contrary, at 180 K an inverse process takes place, where the previously isolated atoms grow onto the droplet. Additionally some Na_2 dimers may be spontaneously formed, and briefly destroyed, during the simulation. This further increases the average fragment size.

D. Electric field

The experiments performed by Dugourd and coworkers²⁹ involve the clusters travelling through a small but very intense region of active electric field. Actually, both the field and its gradient are strong. Because the C and Na atoms get charged differently when put into contact in Na_nC_{60} they may react differently in presence of such a strong field. We attempted to quantify these effects by carrying out extra global optimization for Na_2C_{60} within a field of constant magnitude $E = 5 \times 10^{-4}$ au, corresponding to 2.55×10^8 V m⁻¹. In addition to the 4 atomic degrees of freedom (neglecting the radial distance to the carbons), the direction of the field must also be optimized. Using this approach we found 3 isomers to be potentially the most stable when E is varied between 0 and 10^{-3} au. These isomers are represented in Fig. 8 along with the variations of their energies with increasing field. In isomers B and especially C the two alkali atoms get closer to each other. This is not surprising, since the presence of a strong electric field causes the positively charged ions to move in its direction. As a matter of fact, the field is optimally perpendicular to Na_2 in both B and C, while it has little effect when fully aligned (isomer A). Above $E \sim 10^{-4}$ au, isomer B becomes the most stable until E reached 2.5×10^{-4} , above which C is the new global minimum.

The present results therefore show that a strong, external electric field similar to the one used in experiments can indeed induce some configurational changes in the structure of Na_n adsorbed on C_{60} . Of special interest to us, the field tends to favor metallic bonding by lowering the effects of ionic repulsion. Hence we can expect the onset of nucleation to be earlier in the presence of a field.

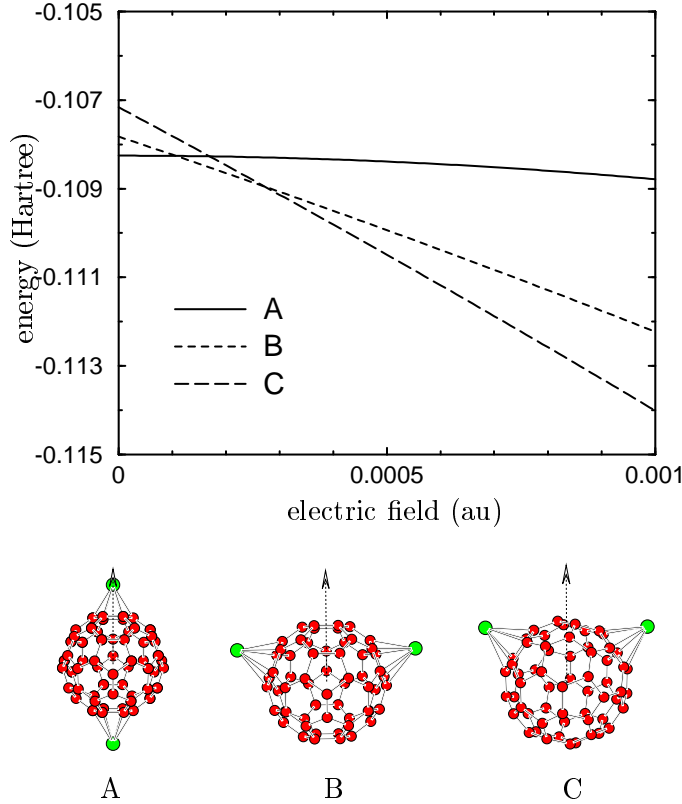


FIG. 8: Variations of the binding energy of three isomers Na_2C_{60} versus the magnitude of electric field. The isomers (A, B, and C) are represented on the lower panel, the arrow indicates the optimal field direction.

E. Dynamics

For each temperature in the range $50 \text{ K} < T < 300 \text{ K}$ with steps $\Delta T = 50 \text{ K}$, we have performed 5000 short (10 ps long) MD trajectories from which we computed the average atomic mean square displacement, and subsequently the diffusion constant D . This was repeated for a number of sizes, and also for a non-zero external electric field. The data for $n = 1, 4, 6, 12,$ and 20 are represented as an Arrhenius plot in Fig. 9. The general linear variations of $\log D$ versus $1/T$ are characteristic of diffusive motion. The activation barriers extracted from these plots are approximately $A \sim 400 \text{ K}$ at zero field, and $A \sim 600 \text{ K}$ at $E = 5 \times 10^{-4} \text{ au}$. At room temperature sodium atoms thus show a significant mobility, whatever a droplet is present or not. Adding an electric field acts as a quench of the dynamics which could trap the system into metastable configurations, provided that the vibrational modes of C_{60} take a part of the excess energy.

V. DISCUSSION AND CONCLUSION

In this work, we have performed *ab initio* and DFT calculations on NaC , NaC_{60} and Na_2C_{60} in order to construct an empirical model for larger clusters. This model allowed us to achieve unconstrained global optimization as well as (thermo)dynamical investigations in a broad size range. Our main findings are as follows:

1. Based on first-principles calculations, Na_2 is most stable in dissociated form, the two sodium atoms lying on opposite hexagonal sites of the fullerene;
2. In its initial stages, the growth of Na_n on C_{60} occurs by minimizing Coulomb repulsion between the nearly cationic alkali atoms, thus placing them as far as possible from each other;
3. At $n \sim 8$, the electrostatic penalty is overcome by creating metallic bonds, and a sodium droplet is formed. The droplet grows for larger sizes;

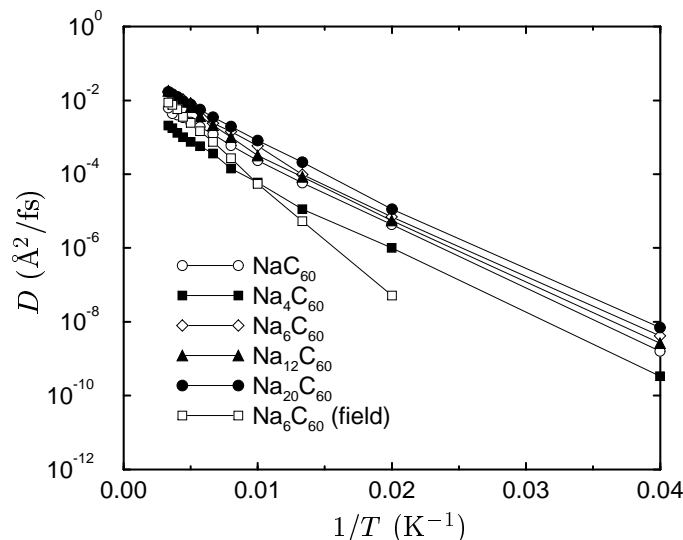


FIG. 9: Diffusion constants of various Na_nC_{60} clusters versus inverse temperature. For Na_6C_{60} , the results of simulations with non-zero external electric field are also plotted for comparison.

4. Depending on the ionic nature of the cluster, the crossover between homogeneous coating and droplet formation varies from 3 (anion) to 10 (cation);
5. A finite temperature or a finite external electric field can enhance metallic bonding and further decrease the crossover size;
6. At room temperature, the alkali atoms undergo a significant mobility over the C_{60} surface.

From these results, a two-stage coating process emerges. This picture is consistent with the observations by the Martin group¹⁸ and by Palpant *et al.*^{26,28} who interpreted their mass spectrometry and photoelectron spectroscopy data as the signature of homogeneous coating at low sizes. However, in accordance with the electric susceptibility measurements by Dugourd and coworkers,²⁹ we find that larger clusters are more stable when they form a droplet. Actually, we predict that Na_nC_{60} clusters with $10 < n < 30$ show an intermediate structure, which consists of a main droplet and some remaining isolated atoms.

Even though the empirical model was parameterized on *ab initio* calculations and experimental data on small clusters, it is nothing more than a model, and should thus be considered as an approximation, especially when used for larger clusters. Therefore, it may well be that the transition between wetted and non-wetted forms takes place at slightly different size if we include other effects such as polarization, or if we describe metallic bonding using a more realistic Hamiltonian such as tight-binding. Also, the existence of rather large sodium coverage of opposite isolated atoms, which mainly results from electrostatic balance in avoiding too large dipole moments, might disappear if more realistic screening due to polarization forces or quantum effects is involved. This is to be further checked.

Nevertheless our conclusions help in solving the experimental puzzling results of various authors. Furthermore, it is remarkable that very recent photodissociation and photoionization experiments carried out by Pellarin and coworkers⁸¹ on the same systems reached the same qualitative *and* quantitative conclusions as ours. At low coverage ($n \leq 6$) they observe ionic-like bonding and strong charge transfer. As the number of metal atoms increases, metallic bonds appear and become preponderant, finally controlling cluster properties. The picture of a metallic cluster deposited on the C_{60} molecule is supported by the odd-even alternation seen in the stability pattern, where even (resp. odd) clusters evaporate mostly single atoms (resp. dimers).

The latter effect is essentially quantum mechanical and lies beyond the empirical potential described in the present work. The favored formation of trimers at low coverage, suggested by Palpant and coworkers²⁸ and further supported by the calculations of Hamamoto *et al.*,¹⁶ is not reproduced here. This is partially due to the neglect of quantum effects, but also to the strong electrostatic repulsion between the alkali atoms. At the onset of nucleation, a trimer is actually formed, which lies perpendicular to the C_{60} surface. Examination of the partial charges shows that, while the two atoms in contact with C_{60} are significantly positively charged, the most outer atom is charged negatively, therefore enhancing the stability of the trimer. It would be interesting to check whether this effect is also seen in electronic structure calculations.

Finally, we would like to stress that the present model is not limited to simple metals adsorbed on fullerenes. Upon careful parameterization using experimental or first-principles data, it could be suitably modified to treat any

other metal, provided that the specific metallic interaction is taken into account. It could also be used for other materials, which are of experimental or technological interest. For instance, the single-crystal X-ray structure of $C_{60}F_{48}$ determined by Troyanov and coworkers⁷⁰ could be reproduced using a similar bond-order potential including fluctuating charges by Stuart *et al.*⁷³ More generally, it is appropriate for treating complex systems, which involve partially covalent and metallic bonding where ionic effects and charge transfer can prove to be a determining factor.

Acknowledgments

The authors wish to thank Ph. Dugourd, M. Broyer, and M. Pellarin for useful discussions. FC thanks F. Rabilloud for help with the Tersoff potential.

APPENDIX: DETAILS OF THE CONFIGURATION INTERACTION CALCULATION FOR NaC

Some information about the distance dependence of the interaction between Na and C in NaC_{60} can be extracted from the NaC molecule. This must however be done with care, since charge transfer is intricately mixed with the multiplet structure of carbon. In order to get a global picture, we have thus determined not only the ground state but also the lowest valence excited states.

The calculation was done representing both C and Na via standard valence semi-local pseudopotentials of the Barthelat and Durand type⁷⁴ with $[1s^2]$ and $[1s^22s^22p^6]$ cores respectively. The calculation was carried out within the Linear Combination of Atomic Orbitals (LCAO) expansion scheme with uncontracted gaussian type functions, namely $5s/5p/5d$ on both centers in order to describe the valence electrons. A core polarization operator of the form $-1/2\alpha_c\vec{f}_c\vec{f}_c$ was added on the sodium core in order to take into account the core-valence polarization and correlation following to the formulation of Müller and Meyer⁷⁷ for the electronic contribution to the electric field \vec{f} on sodium. The Na^+ core polarizability was $\alpha_c = 0.995 a_0^3$, and a unique stepwise cut-off radius⁷⁶ of $1.45 a_0$ was used. The core-polarization contribution on carbon was neglected due to the extremely small value of the dipole polarizability of the C^{4+} ion with respect to that of Na^+ .

The CI treatment was achieved using the multi-reference variational-perturbative CI algorithm CIPSI⁸⁰ within its Quasi-Degenerate Perturbation Theory version⁷⁹ and the Möller-Plesset partition of the Hamiltonian. The intermultiplet separations of the carbon atom, calculated consistently, were found to be $\Delta(^3P-^1D)=1.386$ eV, $\Delta(^3P-^1S)=2.565$ eV, versus 1.260 and 2.680 eV experimentally.⁷⁸ For C^- the separations were found to be $\Delta(^4P-^2D)=1.656$ eV, $\Delta(^4P-^2S)=2.095$ eV.

The lowest states potential energy curves are shown in Fig. 10. Combination of $Na(3s^2S)$ with $C(^3P)$ generates three molecular states, namely $1^4\Sigma^-$, $1^2\Sigma^-$ and $1^2\Pi$. Combination with $C(^1D)$ also generates three states, namely $1^2\Delta^-$, $2^2\Pi$ and $1^2\Sigma^+$. Finally, combination with $C(^1S)$ generates a single state $2^2\Sigma^+$. In the following, the valence molecular orbitals (MO's) will be labelled 1σ , 2σ , 3σ , $1\pi_x$, and $1\pi_y$. Despite hybridization, they can be qualitatively associated with the $2s$, $2p_z$, $3s$, $2p_x$ and $2p_y$ atomic orbitals, respectively.

The ground molecular state correlated with the $C(^3P)$ asymptote is a quartet state, $1^4\Sigma^-$. At its equilibrium distance $R_e=4.40 a_0$, it is mainly spanned by molecular configuration $1\sigma^22\sigma^11\pi_x^1\pi_y^1$ with all the electrons in the $2p$ shell of carbon and is therefore expected to be strongly ionic. The DFT-B3LYP calculation of the NaC ground state provides very similar results, see Fig. 10. In particular, the dipole moment is found to be 7.88 D at the equilibrium distance. This is confirmed by the dipole moment value $\mu = 8.53$ D at the equilibrium distance and the associated charge transfer $\delta q = 0.80$. It can be clearly seen in Fig. 10 that the ground state adiabatically undergoes at $R = 7.6 a_0$ a strong avoided crossing with a state of same symmetry $2^4\Sigma^-$. As a consequence of the configuration switch, the adiabatic state $2^4\Sigma^-$ has a small dipole moment in the short distance range $R < 6 a_0$. In the long distance range $10 a_0 < R < 14 a_0$, it is correlated with $C(^4P) + Na^+$ and its potential curve exhibits a $-1/R$ behavior, consistent with a continuously increasing dipole moment (up to $\mu \approx -21.6$ D at $R = 12 a_0$, the value for a perfectly ionic state would be -30.5 D). For still larger distances, the state interacts with another covalent excited state. The strong coupling between the two quartet states $1^4\Sigma^-$ and $2^4\Sigma^-$ states explains the significant dissociation energy of the ground state $D_e = 1.464$ eV.

Most other states dissociating into neutral asymptotic limits show similar (sometimes multiple) avoided crossing, mainly due to their interaction with ionic configurations. The positions of the avoided crossings are obviously determined by the respective positions of the multiplets of carbon and those of the ionic states dissociating into $C^- + Na$. This also influences the dissociation energies of the lowest states stabilized by the interactions. In consistency with this picture, one can notice the avoided crossing between states $1^2\Sigma^-$ and $2^2\Sigma^-$, those between the three $2^2\Pi$ states and finally that between $1^2\Delta$ and $2^2\Delta$. As a result, the lowest states involved in the avoided crossings are stabilized. This leads to significant dipole moments and charge transfer values at equilibrium for two other states correlated with the

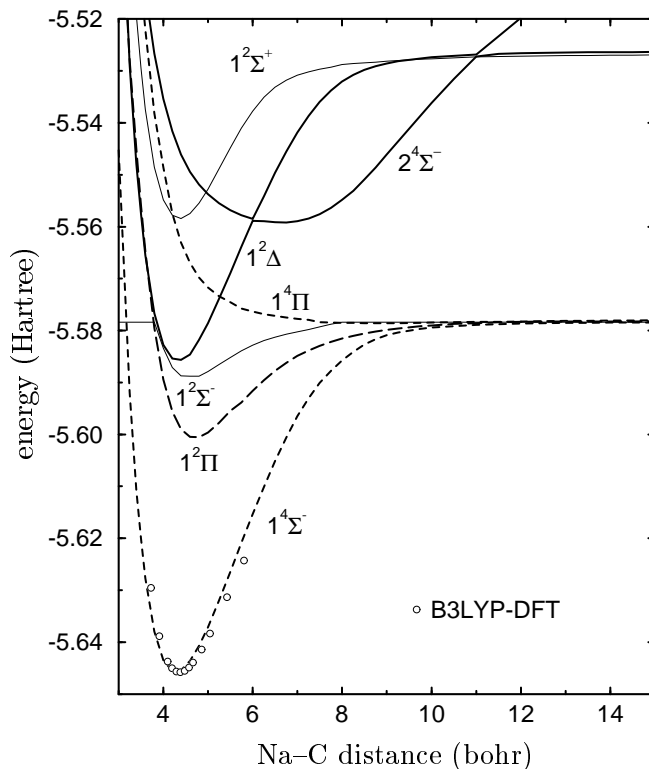


FIG. 10: Potential energy curves of the NaC molecule. All continuous curves correspond to CI calculations. Some DFT values are also reported (dots) for the ground state.

lowest asymptote, and explains their bonding properties ($D_e = 0.30$ eV, $R_e = 4.6 a_0$ for state $1^2\Sigma^-$, $D_e = 0.60$ eV, $R_e = 4.7 a_0$ for state $1^2\Pi$). The same holds for state $1^2\Delta$ ($D_e = 1.61$ eV, $R_e = 4.4 a_0$) dissociating into C(1D). State $1^4\Pi$ is the only exception to the previous behavior, since it is spanned by configuration $1\sigma^2 2\sigma^1 1\pi_x^1 1\pi_y^2 3\sigma^1$. Indeed within a single configuration approximation, no charge transfer can take place between the 2σ and 3σ MO's in the quartet state because all singly occupied orbital spins are aligned. This state can thus be described as essentially covalent with a weak dipole moment and small charge transfer ($\delta q = 0.25$ at $R = 4 a_0$). Its potential curve is essentially non bonding and can be fitted via a simple exponential form, which can be used as the NaC covalent repulsive term of the model, Eq. (4).

-
- ¹ *Recent Advances in the Chemistry and Physics of Fullerenes and Related Materials*, K. M. Kadish and R. S. Rinoff editors, The Electrochemical Society, Inc., Washington DC, 1998, Vol 6.
- ² A. F. Hebard, M. J. Rosseinsky, R. C. Haddon *et al.*, *Nature (London)* **350**, 600 (1991).
- ³ G. Oszlányi, G. Baumgartner, G. Faigel, and L. Forró, *Phys. Rev. Lett.* **78**, 4438 (1997).
- ⁴ Y. Kubozono, Y. Takabayashi, S. Fujiki, S. Kashimo, T. Kambe, Y. Iwasa, and S. Emura, *Phys. Rev. B* **59**, 15 062 (1999).
- ⁵ J. Kohanoff, W. Andreoni, and M. Parrinello, *Chem. Phys. Lett.* **198**, 472 (1992).
- ⁶ D. Östling and A. Rosén, *Chem. Phys. Lett.* **202**, 389 (1993).
- ⁷ A. Rubio *et al.*, *Phys. Rev. B* **49**, 17 397 (1994).
- ⁸ A. S. Hira and A. K. Ray, *Phys. Rev. A* **52**, 141 (1995).
- ⁹ A. S. Hira and A. K. Ray, *Phys. Rev. A* **54**, 2205 (1996).
- ¹⁰ M. Springborg, S. Satpathy, N. Malinowski, U. Zimmermann, and T. P. Martin, *Phys. Rev. Lett.* **77**, 1127 (1996).
- ¹¹ D. Östling and A. Rosén, *Chem. Phys. Lett.* **281**, 352 (1992).
- ¹² T. Aree, T. Kerdchaoren, and S. Hannongbua, *Chem. Phys. Lett.* **285**, 221 (1998).
- ¹³ Z. Slanina, C. Miyajama, X. Zhao, L. Adamowicz, and E. Osawa, *Comp. Mater. Sci.* **18**, 308 (2000).
- ¹⁴ X. G. Gong and V. Kumar, *Chem. Phys. Lett.* **334**, 238 (2001).
- ¹⁵ P. Mierzyński and K. Pomorski, *Euro. Phys. J. D* **21**, 311 (2002).
- ¹⁶ N. Hamamoto, J. Jitsukawa, and C. Satoko, *Euro. Phys. J. D* **19**, 211 (2002).
- ¹⁷ L.-S. Wang, O. Cheshnovsky, R. E. Smalley, J. P. Carpenter, and S. J. Hwo, *J. Chem. Phys.* **96**, 4028 (1992).

- ¹⁸ T. P. Martin, N. Malinowski, U. Zimmermann, U. Näher, and H. Schaber, *J. Chem. Phys.* **99**, 4210 (1993).
- ¹⁹ U. Zimmermann, N. Malinowski, U. Näher, S. Frank, and T. P. Martin, *Phys. Rev. Lett.* **72**, 3542 (1994).
- ²⁰ P. Weis, R. D. Beck, G. Bräuchle, and M. M. Kappes, *J. Chem. Phys.* **100**, 5684 (1994).
- ²¹ U. Zimmermann, A. Burkhardt, N. Malinowski, U. Näher, and T. P. Martin, *J. Chem. Phys.* **101**, 2244 (1994).
- ²² U. Zimmermann, N. Malinowski, A. Burkhardt, and T. P. Martin, *Carbon* **33**, 995 (1995).
- ²³ F. Tast, N. Malinowski, M. Heinebrodt, I. M. L. Billas, and T. P. Martin, *J. Chem. Phys.* **106**, 9372 (1997).
- ²⁴ S. Frank, N. Malinowski, F. Tast, M. Heinebrodt, I. M. L. Billas, and T. P. Martin, *Z. Phys. D.* **40**, 250 (1997).
- ²⁵ J. L. Fye and M. F. Jarrold, *Int. J. of Mass. Spect.* **187**, 506 (1999).
- ²⁶ B. Palpant, A. Otake, F. Hayakawa, Y. Negishi, G. H. Lee, A. Nakajima, and K. Kaya, *Phys. Rev. B* **60**, 4509 (1999).
- ²⁷ D. Rayane, R. Antoine, Ph. Dugourd, E. Benichou, A. R. Allouche, M. Aubert-Frécon, and M. Broyer, *Phys. Rev. Lett.* **84**, 1962 (2000).
- ²⁸ B. Palpant, Y. Negishi, M. Sanekata, K. Miyajima, S. Nagao, K. Judai, D. M. Rayner, B. Simard, P. A. Hackett, A. Nakajima, and K. Kaya, *J. Chem. Phys.* **114**, 8549 (2001).
- ²⁹ Ph. Dugourd, R. Antoine, D. Rayane, I. Compagnon, and M. Broyer, *J. Chem. Phys.* **114**, 1970 (2001).
- ³⁰ H. Tanaka, S. Osawa, J. Onoe, and K. Takeuchi, *J. Phys. Chem. B* **103**, 5939 (1999).
- ³¹ M. Ohara, Y. Nakamura, Y. Negishi, K. Miyajima, A. Nakajima, and K. Kaya, *J. Phys. Chem. A* **106**, 4498 (2002).
- ³² Some of the results presented here have appeared in our previous article, *Phys. Rev. Lett.* **90**, 075505 (2003).
- ³³ A. D. Becke, *Phys. Rev. A* **38**, 3098 (1988).
- ³⁴ C. Lee, W. Yang, and R. G. Parr, *Phys. Rev. B* **37**, 785 (1988).
- ³⁵ A. D. Becke, *J. Chem. Phys.* **98**, 5648 (1993).
- ³⁶ M. J. Frisch *et al.*, GAUSSIAN 98 Revision A.6, Gaussian Inc., Pittsburgh P.A, 1998.
- ³⁷ C. Lee, W. Yang, and R. G. Parr, *Phys. Rev. B* **37**, 785 (1988).
- ³⁸ P. J. Hay and W. R. Wadt, *J. Chem. Phys.* **82**, 284 (1985).
- ³⁹ K. Hedberg, L. Hedberg, D. S. Betlume, C. A. Brown, H. C. Dorn, R. D. Johnson, and M. d. Vries, *Science* **254**, 410 (1991).
- ⁴⁰ R. Antoine, D. Rayane, E. Benichou, Ph. Dugourd, and M. Broyer, *Euro. Phys. J. D* **12**, 147 (2000).
- ⁴¹ A. D. Becke, *Phys. Rev.* **33**, 2786 (1986).
- ⁴² R. S. Mulliken, *J. Chem. Phys.* **23**, 1833 (1955).
- ⁴³ W. J. Mortier, K. V. Genechten, and J. Gasteiger, *J. Am. Chem. Soc.* **107**, 829 (1985); W. J. Mortier, S. K. Ghosh, and S. Shankar, *ibid.* **108**, 4315 (1986).
- ⁴⁴ A. K. Rappé and W. A. Goddard, III, *J. Phys. Chem.* **95**, 3358 (1991).
- ⁴⁵ S. Sawada and S. Sugano, *Z. Phys. D: At. Mol. Clusters* **20**, 259 (1991).
- ⁴⁶ S. W. Rick, S. J. Stuart, and B. J. Berne, *J. Chem. Phys.* **101**, 6141 (1994).
- ⁴⁷ R. Car and M. Parrinello, *Phys. Rev. Lett.* **55**, 2471 (1985).
- ⁴⁸ D. M. York and W. Yang, *J. Chem. Phys.* **104**, 159 (1996).
- ⁴⁹ P. Istkowitz and M. L. Berkowitz, *J. Phys. Chem. A* **101**, 5687 (1997).
- ⁵⁰ M. J. Field, *Molec. Phys.* **91**, 835 (1997).
- ⁵¹ H. A. Stern, F. Rittner, B. J. Berne, and R. A. Friesner, *J. Chem. Phys.* **115**, 2237 (2001).
- ⁵² F. Calvo, *Phys. Rev. B* **67**, 161403(R) (2003).
- ⁵³ M. C. C. Ribeiro, *Phys. Rev. B* **61**, 3297 (2000); **63**, 094205 (2001).
- ⁵⁴ M. C. C. Ribeiro, *J. Chem. Phys.* **117**, 266 (2002).
- ⁵⁵ F. Ducastelle, *J. Phys. (Paris)* **31**, 1055 (1970).
- ⁵⁶ Y. Li, E. Blaisten-Barojas, and D. A. Papaconstantopoulos, *Phys. Rev. B* **57**, 15 519 (1998).
- ⁵⁷ J. Tersoff, *Phys. Rev. Lett.* **61**, 2879 (1988).
- ⁵⁸ T. I. Schelkacheva and E. E. Tareyeva, *Phys. Rev. B* **61**, 3143 (2000).
- ⁵⁹ K. Ohno, *Theor. Chim. Acta* **2**, 219 (1964).
- ⁶⁰ R. T. Sanderson, *Science* **114**, 670 (1951).
- ⁶¹ G. H. Jeung, *J. Phys. B* **16**, 4289 (1983).
- ⁶² R. Antoine, Ph. Dugourd, D. Rayane, E. Benichou, M. Broyer, F. Chandezon, and C. Guet, *J. Chem. Phys.* **110**, 9771 (1999).
- ⁶³ Z. Li and H. A. Scheraga, *Proc. Natl. Acad. Sci. USA* **84**, 6611 (1987).
- ⁶⁴ D. J. Wales and J. P. K. Doye, *J. Phys. Chem. A* **101**, 5111 (1997).
- ⁶⁵ G. J. Martyna, M. L. Klein, and M. Tuckerman, *J. Chem. Phys.* **97**, 2635 (1992).
- ⁶⁶ M. Sprik, *J. Phys. Chem.* **95**, 2283 (1991).
- ⁶⁷ R. H. Swendsen and J.-S. Wang, *Phys. Rev. Lett.* **57**, 2607 (1986); G. Geyer, in *Computing Science and Statistics: Proceedings of the 23rd Symposium on the Interface*, E. K. Keramidis ed. (Interface Foundation, Fairfax Station, 1991), p. 156.
- ⁶⁸ W. D. Knight, K. Clemenger, W. de Heer, W. A. Saunders, M. Y. Chou, and M. L. Cohen, *Phys. Rev. Lett.* **52**, 2141 (1984).
- ⁶⁹ S. G. Kim and D. Tománek, *Phys. Rev. Lett.* **72**, 2418 (1994).
- ⁷⁰ S. I. Troyanov, P. A. Troshin, O. V. Boltalina, I. N. Ioffe, L. N. Sidorov, and E. Kemnitz, *Angew. Chem. Int. Ed.* **40**, 2285 (2001).
- ⁷¹ F. Calvo and F. Spiegelmann, *Phys. Rev. Lett.* **82**, 2270 (1999).
- ⁷² A. M. Ferrenberg and R. H. Swendsen, *Phys. Rev. Lett.* **61**, 2635 (1988).
- ⁷³ S. Stuart (private communication).
- ⁷⁴ J. C. Barthelat and Ph. Durand, *Theoret. Chim. Acta* **38**, 283 (1975).
- ⁷⁵ T. H. Dunning and P. J. Hay, *Modern Theoretical Chemistry*, ed. H. F. Schaefer III (Plenum, New York), vol. 3, p. 1, 1976.

- ⁷⁶ M. Foucrault, Ph. Millié, and J. P. Daudey, *J. Chem. Phys.* **96**, 1257 (1992).
- ⁷⁷ W. Müller, J. Flesch, and W. Meyer, *J. Chem. Phys.* **80**, 3297 (1984); W. Müller and W. Meyer, *J. Chem. Phys.* **80**, 3311 (1984).
- ⁷⁸ C. E. Moore, *Atomic Energy Levels*, Circular 467, vol I, NBS, US Dept. of Commerce (1952).
- ⁷⁹ F. Spiegelmann and J. P. Malrieu, *J. Phys. B* **17**, 1235 (1984).
- ⁸⁰ B. Huron, J. P. Malrieu, and P. Rancurel, *J. Chem. Phys.* **58**, 5745 (1973).
- ⁸¹ M. Pellarin, E. Cottancin, J. Lermé, J. L. Vialle, M. Broyer, F. Tournus, B. Masenelli, and P. Mélinon, *Euro. Phys. J. D.* (in press, 2003).